Design of Mott and topological phases on buckled $3d$-oxide honeycomb lattices

David Doennig,[1] Warren E. Pickett,[2] and Rossitza Pentcheva[3, 1, *]

[1] *Forschungs-Neutronenquelle Heinz Maier-Leibnitz (FRM II), Technische Universität München, Lichtenbergstraße 1, 85748 Garching, Germany*

[2] *Department of Physics, University of California Davis, One Shields Avenue, Davis, CA 95616, U.S.A.*

[3] *Department of Physics and Center for Nanointegration Duisburg-Essen (CENIDE), University of Duisburg-Essen, Lotharstr. 1, 47057 Duisburg, Germany*

(Dated: July 16, 2015)

Digital oxide heterostructures – materials grown layer-by-layer – have demonstrated promise for electronics and spintronics device applications due to emergent electronic phases, ranging from high mobility two-dimensional (2D) spin-polarized electron gases to magnetism and superconductivity. Beyond the heavily studied (001) crystallographic orientation, topological and perhaps more exotic phenomena are expected in (111)-oriented perovskite bilayers due to the key structural aspect of a buckled honeycomb ("graphene") lattice. To identify prospective materials realizations, density functional studies including on-site Coulomb repulsion render a comprehensive picture of the evolution of ground states versus band filling in (111)-oriented $(LaXO)_2/(LAO)_4$ superlattices, with X spanning the entire $3d$ transition metal series, incorporating the complexities of multiorbital open shell cations. We find unanticipated broken symmetry phases to be ubiquitous, with mechanisms ranging from Jahn-Teller distortions, to charge-, spin-, and orbital-ordering. $LaMnO_3$ and $LaCoO_3$ bilayers, where spin-orbit coupling additionally gaps the Dirac point Fermi surface, emerge as promising candidates signaling a possible transition between a trivial Mott and a topological insulator phase.

PACS numbers: 73.21.Fg, 73.22.Gk, 75.70.Cn

INTRODUCTION

Synthesis and characterization of atomically abrupt transition metal oxide (TMO) heterostructures has revealed a broad platform of unanticipated functionalities and has fueled widespread expectation that such systems will impact and enhance next generation electronics and spintronics capabilities by controlling charge, spin, orbital, and lattice degrees of freedom at the nanoscale.[1, 2]

The earlier focus on perovskite materials with the (001) growth orientation - prominent examples here being e.g. the interface between $LaAlO_3$ and $SrTiO_3$ (LAO/STO)[3, 4] or nickelate superlattices [5] - has recently been extended to the (111) orientation.[6, 7] In the latter, two triangular BO_6 sublattices form a buckled honeycomb lattice topologically equivalent to graphene. The honeycomb lattice itself introduces exotic possibilities. Considering an alternating, next nearest neighbor (nnn) *imaginary* hopping amplitude, Haldane modeled a quantum spin Hall (QSH) system without explicit external field.[8] In the Kane-Mele elucidation[9] of the honeycomb lattice, topological behavior originated from spin-orbit coupling (SOC) entanglement of band character. Later, Raghu *et al.*[10] proposed that topological character can be generated by strong interactions (even in the mean field approximation). Wright generalized Haldane's model to a *buckled honeycomb lattice* in which magnetic flux, alternating in orientation in neighboring cells, leads to a Chern (quantum anomalous Hall [QAH]) insulator[11] with topologically protected gapless edge states. These specific models are, however, challenging to realize in real materials.

Compared to graphene and common topological insulators (TI), TMOs possess not only larger band gaps, but offer an enormously richer palette of possibilities due to several distinctive features: correlated electron behavior causing spin, charge, and orbital instabilities, multiorbital configurations on each of the sublattices combined with relativistic effects, viz. spin-orbit coupling. Below we extend this already substantial set of possibilities to include band filling as well, and show that an interplay of strong interactions and SOC effects, which operate in the $3d$ 111 bilayers with their buckled honeycomb lattice, produce specific spin-fermion systems as candidates for QSH or QAH systems.

The idea of constructing a (111) bilayer from perovskite TMO was initially introduced by Xiao *et al.* for $4d$ and $5d$ e_g systems, pointing to possibilities for "interface engineering of quantum anomalous Hall effects.[12] Building on this foundation, Yang *et al.*[13] and Rüegg and Fiete[14] constructed a tight-binding (TB) model for $(LaNiO_3)_2$/LAO, and demonstrated that in certain ranges of parameters and magnetic order topological insulating phases can result from ordering involving a complex combination of e_g orbitals.[14] Recently, Cook and Paramekanti[15] suggested double perovskites as a potential system to realize the model Chern insulator, as proposed by Wright,[11] but experimental verification of any QAH insulator has been lacking.

Complementary to tight-binding models, material-specific density functional theory (DFT) is essential to

achieve a fundamental understanding and to predict actual materials realizations. Besides examples for $5d$ systems[16], DFT studies including strong local interaction effects (see below) have recently predicted a Dirac point Fermi surface for a STO(111)[17] and LNO(111) bilayers, quantum confined within LAO.[13, 14, 18–20] In these cases the Dirac point is 'protected' by symmetry; sublattice symmetry breaking leads to gap-opening charge-disproportionated states.[17, 19]

To identify further promising systems as well as to elucidate the underlying *design principles* of functionalities, we have explored systematically the effect of band filling on the electronic ground state in (111) oriented $(\mathrm{La}X\mathrm{O}_3)_2/(\mathrm{LaAlO}_3)_4$ superlattices, where X spans the range of trivalent $3d$ ions Ti-Cu. Despite the fact that these systems, unlike LAO/STO(111), are nonpolar - i.e. there is no valence mismatch across the interface, so all transition metal cations retain X^{3+} configurations - unexpected phases proliferate. Competition between local pseudocubic symmetry and global trigonal symmetry as well as additional flexibility, provided by the magnetic and spin degrees of freedom of $3d$ ions, lead to a broad array of distinctive broken symmetry ground states, offering a platform to design 2D electronic functionalities.[21]

TRENDS ACROSS THE $3d$ SERIES

A central aspect in the $(\mathrm{La}X\mathrm{O}_3)_2/(\mathrm{LaAlO}_3)_4(111)$ honeycomb bilayers is their strong deviation from their bulk analogs. Certain recurring features tied to the t_{2g} and e_g distinction can be identified, thus we discuss them separately.

t_{2g} systems

For the t_{2g} subshell the dominating feature is a competition between local pseudo-cubic symmetry and the underlying threefold+inversion symmetry ("P321") of the ideal bilayer. The (111) bilayering reduces the octahedral symmetry to trigonal and splits the t_{2g} orbital triplet into $a_{1g} + e'_g$, with the former having zero angular momentum around the $\hat{c}$ bilayer axis while the latter orbital doublet forms a representation for $m_\ell = \pm 1$ angular momentum with corresponding orbital orientation and shape. Breaking this symmetry allows occupation of the cubic d_{xy}, d_{yz}, or d_{xz} orbitals.

$\underline{X{=}\mathrm{Ti}^{3+}\ 3d^1}$. The above scenario arises most vividly for the LaTiO_3 bilayer, which displays the richest behavior among the t_{2g} systems. The ground state, pictured in Fig. 1a), at a_{LAO} is a ferromagnetic (FM) orbitally ordered Mott insulator, displaying staggered d_{xz}, d_{yz} occupation and a very narrow (0.2 eV bandwidth) lower Hubbard band. This is in contrast to bulk LaTiO_3 which is a distorted $Pbnm$, G-type antiferromagnetic (AFM) Mott insulator with $1/\sqrt{3}(d_{xy} + d_{yz} + d_{zx})$ orbital order [26, 27]. Consistent with this extremely localized character, the corresponding AFM state with the same orbital polarization, shown in Fig. 1e, is only 4 meV/u.c. higher in energy, suggesting a weak exchange coupling of $\sim$1 meV.

Constraining the symmetry to P321, thereby keeping the two Ti ions related by symmetry, results in e'_g orbital polarization with bands touching at K and K′ (Fig. 1f). This degeneracy protects the system against the Mott insulating gap, presenting an unusual case of strong correlation effects are being rendered ineffectual by an imposed symmetry. Despite its high energy cost (0.4 eV/Ti), this state is intriguing due to the unusual direction reversal of bands in the vicinity of K and K′ points (note zoom-in of the band structure in Fig. 1g). This intertwining of the bands suggests topological character.

Inclusion of SOC for magnetization along [001] for this case leads to a band inversion and a resulting gap (green line in Fig. 1g). The points K and K′ become inequivalent. This signals the loss of equivalence of the two Ti ions, reflected in an surprisingly large orbital moment of one of the ions: $0.11\mu_B$ versus just $0.01\mu_B$ on the other.

Ti orbital polarization is highly susceptible to strain tuning: Applying tensile strain by imposing the lateral lattice constant of a_{STO} tips the pseudo-cubic/trigonal symmetry balance, stabilizing occupation of the a_{1g} orbital (Fig. 1h). The band structure just below the gap is comprised of two filled bands with Dirac crossings at K and K′, similar to the analogous LAO/STO(111) case.[19] While in the latter case the $3d^{0.5}$ band filling puts the Dirac points at E_{F}, here both bands are fully occupied.

$\underline{X = \mathrm{V}^{3+}\ 3d^2}$. The AFM ground state of the LaVO_3-bilayer, displayed in Fig. 1b, is gapped due to occupation of the e'_g doublet. This is insensitive to strain and at variance with the bulk G-type d_{xz}, d_{yz} orbital ordering (d_{xy} is occupied on all sites)[27, 28]. Thus in this LaVO_3 bilayer trigonal symmetry splitting dominates over the pseudocubic crystal field. The spin-aligned FM state (Fig. 1c) with the same orbital polarization is 73 meV/u.c. higher in energy, and has four bands topologically similar to those of the metastable $2\mathrm{LaTiO}_3$ case (Fig. 1f), with the difference that now the entire set of bands is filled.

$\underline{X = \mathrm{Cr}^{3+}\ 3d^3}$. The Cr bilayer is electronically trivial: a half-filled t_{2g}-band ($t^3_{2g,\uparrow}$, S=$\frac{3}{2}$), thus no orbital degrees of freedom, and antiferromagnetic order (Fig. 1d).

e_g systems

Consistent with the tight-binding model of Xiao *et al.*[12] a distinctive set of four bands emerges for ferromagnetic coupling for an open e_g subshell: nearly flat bottom and top bands interconnected by two dispersive

FIG. 1: Electronic ground (a-d) and selected metastable (e-h) states in $(LaXO_3)_2/(LaAlO_3)_4(111)$ for t_{2g} systems X=Ti, V, Cr. Shown are the band structures with blue/orange denoting the majority/minority bands, and isosurfaces of the spin density, with majority in blue and minority in red. In cases (a,e,h) the integration range was adapted to emphasize the orbital polarization. Energies of metastable states are provided in red.

FIG. 2: Presentation as in Fig. 1, but for e_g systems X=Mn, Fe, Co, Ni, and Cu. A striking feature is the similarity in band structure of X=Mn, Co, Ni, despite the formal different band filling: a Dirac point Fermi surface within P321 (a)-(c) and a gap opening due to symmetry breaking. The ground state results are presented in (d)-(h).

bands, providing a Dirac point crossing at the K and K′ points and quadratic contact with the flat bands at the Γ point (cf. Fig. 2a-c,h,l). Band filling together with the orbital and spin degrees of freedom determine the position of the Dirac point with respect to the Fermi level. Equivalence of the two sublattices again becomes crucial. This symmetry is found to be broken in all e_g system ground states where the Dirac point is initially at the Fermi level. We identify distinct origins of symmetry breaking and the resulting gap opening in each system, as discussed below.

X=Mn^{3+} $3d^4$. The $LaMnO_3$ bilayer provides one of the promising cases where, within P321 symmetry, the system exhibits a Dirac point Fermi surface within the e_g bands (Fig.2a). The Mn ion ($t^3_{2g,\uparrow}e^1_{g,\uparrow}$ with the e_g-band quarter-filled) is unstable to Jahn-Teller distortion. Releasing structural symmetry restrictions leads to an elongation of the apical Mn-O bond lengths to 2.07-2.11 Å and variation of the basal distances between 1.89-1.98 Å, associated with alternating $d_{3y^2-r^2}$, $d_{3x^2-r^2}$ occupation on the A and B sublattices (Fig. 2e). This symmetry breaking opens a gap of 0.8 eV and also lifts the quadratic band touching degeneracy at Γ. The Jahn-Teller distortion is also present in the AFM order (Fig. 2i), which is 88 meV/u.c. higher in energy. The much flatter bands reflect electronic decoupling of the two sublattices, similar to the AFM $LaNiO_3$ bilayer (Fig. 2k), discussed below.

X=Fe^{3+} $3d^5$. The ground state of the $LaFeO_3$ bilayer is a high spin (HS) AFM band insulator with nearly spherically symmetric charge and spin density on the Fe site characteristic of a half-filled $3d$ band ($t^3_{2g,\uparrow}e^2_{g,\uparrow}$ with S=$\frac{5}{2}$, cf. Fig 2d). For comparison, bulk $LaFeO_3$ is a G-type AFM with orthorhombic *Pnma* structure. The metastable FM configuration exhibits the previously discussed set of four bands, albeit now these are fully occupied for the majority spin channel (cf. Fig 2l).

X=Co^{3+} $3d^6$. Bulk $LaCoO_3$ has a low spin (LS) (t^6_{2g}) narrow gap insulating ground state, but becomes ferromagnetic e.g. as a strained film [29]. A rich set of (metastable) states with respect to spin degrees of freedom can be anticipated and are indeed realized in the $LaCoO_3$ bilayer. Constraining symmetry to P321 renders another case where the Fermi level is pinned at a Dirac point (Fig. 2b). This state lies 0.21 eV above the broken symmetry ground state of FM intermediate spin (IS) (t^5_{2g}, e^1_g) insulator with a moment of $1.97\mu_B$ (Fig. 2f). Orbital ordering of the e_g electron and t_{2g} hole drives the breaking of symmetry, analogous to the case of Mn but with a smaller band gap.

A further metastable state, only 19 meV less favorable, exhibits a new type of *spin state symmetry breaking* in which the two Co sublattices assume IS and LS states with very flat bands accompanied by (and presumably caused by) a $d_{x^2-y^2}$ orbital occupation on the IS Co sublattice (Fig. 2j).

X=Ni^{3+} $3d^7$. Bulk $LaNiO_3$ is a $R\bar{3}c$ correlated metal. [26]. Within P321 symmetry a Dirac point Fermi surface is obtained (cf. Fig. 2c), as previously reported [13, 18–20] for the $LaNiO_3$ bilayer. However, breaking the equivalency of the two triangular sublattices opens a gap of 0.25 eV at the Fermi level (cf. Fig. 2g)[19]. Here the mechanism is disproportionation of the Ni sublattice, expressed in different magnetic moments of 1.30 and 1.08 μ_B. AFM coupling of the two bilayers results in flat bands (Fig. 2k), defining a band gap of ~ 1 eV with orbital polarization at the Ni sites, as recently observed in a $NdNiO_3$ bilayer.[6] This illustrates how antiferromagnetic order provides the necessary decoupling of the two trigonal bilayers, analogous to the La_2NiAlO_6 double perovskite where the single triangular Ni-layers are separated by Al-layers [19].

X=Cu^{3+} $3d^8$. This case provides a straightforward $e^2_{g,\uparrow}$ S=1 ion at half filling of the e_g bands, with large optical (spin-conserving) gap but with very low energy spin-flip excitations (Fig. 2h, see also Xiao *et al.*[12]). Although Cu^{3+} is uncommon (bulk $LaCuO_3$ is metallic and must be synthesized under pressure),[30] it might be stabilized by non-equilibrium epitaxial synthesis.

Analogies and distinctions. Despite the formal difference in band filling for X=Mn, Co, and Ni, an unexpected analogy occurs in the electronic structure of these bilayers: a Dirac-point Fermi surface when constrained to P321 symmetry reverts to a gapped Mott insulator state, being driven by symmetry breaking forces of distinct origin: a Jahn-Teller distortion in $LaMnO_3$; a spin transition to IS accompanied by orbital order in $LaCoO_3$; and a charge disproportionation in $LaNiO_3$.

Spin-orbit coupling. Generally no significant SOC is expected in the $3d$ series beyond minor band splittings

FIG. 3: Effect of SOC on $(LaXO_3)_2/(LaAlO_3)_4$ a) X=Mn, magnetization along [100]; b) X=Co, magnetization along [100].

and small magnetocrystalline anisotropy. However, an unusually strong effect arises in $LaMnO_3$ and $LaCoO_3$: SOC gaps both the Dirac points at K, K', as well as the quadratic band touching at Γ. $(LaMnO_3)_2$ shows a stronger influence of SOC, with an in-plane [100] easy axis (Fig. 3a), while $(LaCoO_3)_2$ has an out-of plane easy axis (Fig. 3b). The opening of a gap due to SOC suggests a topological phase with a possible transition between the TI state and the Mott insulating state discussed above. Thus the $LaMnO_3$ and $LaCoO_3$ bilayers emerge as candidates for topological insulators.

SUMMARY

Apart from three cases of filled subshells that stabilize symmetric phases, the buckled $3d$ honeycomb bilayers encounter and succumb to a variety of symmetry-breaking forces: (1) orbital ordering including competition between occupation of real pseudocubic orbitals (d_{xy}, d_{xz}, d_{yz} for t_{2g}; $d_{x^2-y^2}$ and d_{z^2} for e_g) and their triangular lattice counterparts; (2) charge disproportionation, (3) spin-state differentiation, and (4) Jahn-Teller distortion.

Spin-orbit coupling, known to be important in $5d$ and even $4d$ transition metal ions, gaps the Dirac point Fermi surface in X=Mn and Co. Further broken symmetries occur, but simply renormalize the gap and redefine the character of the ground state, sometimes in distinctive ways, viz. the spin-state asymmetry for the Co case.

This study outlines the variety of possibilities for unusual ground states and for topological behavior in this "$3d$ palette" of two-dimensional oxide honeycomb lattices. These results should stimulate research on the experimental realization of these phases, which can be combined into numerous hybrid systems using multilayer growth techniques. Doping of these materials provides further possibilities to tune the functionalities for their intrinsic interest as well as for potential applications.

METHODS

DFT calculations were performed on (111)-oriented $(LaXO_3)_2/(LaAlO_3)_4$ superlattices with X ranging throughout the $3d$ series Ti-Cu, using the all-electron full-potential linearized augmented-plane-wave (LAPW) method, as implemented in the WIEN2k code [22]. For the exchange-correlation functional we used the generalized gradient approximation (GGA) [23]. Static local electronic correlations were included in the GGA+U approach [24] with U =5 eV, J =0.7 eV (for all X = Ti-Cu $3d$) and U = 8 eV (La $4f$). Systematic investigations of the influence of U were performed and have shown that the results are robust with respect to variation of the U parameter in a reasonable range of values. Additional calculations with the modified Becke-Johnson [25] potential support the obtained electronic behavior.

The lateral lattice constant is fixed to a_{LAO}=3.79 Å, corresponding to superlattices grown on a LAO(111) substrate, unless otherwise stated. Octahedral tilts and distortions were fully taken into account when relaxing atomic positions, whether constrained to P321 symmetry or fully released to P1 symmetry. Additionally, the out-of-plane lattice parameter c was optimized for all superlattices. Spin-orbit coupling (SOC) was treated using the second-variational method.

R.P. and D. D. acknowledge financial support through the DFG SFB/TR80, project G3. W. E. P. was supported by U.S. Department of Energy Grant No. DE-FG02-04ER46111.

* Electronic address: Rossitza.Pentcheva@uni-due.de

[1] Hwang, H. Y. ,*et al.*, Emergent phenomena at oxide interfaces, *Nat. Mater.* **11**, 103 (2012).
[2] Mannhart, J. & Schlom, D. G., Oxide Interfaces - An Opportunity for Electronics, *Science* **327**, 1607 (2010).
[3] Pentcheva, R. & Pickett, W. E., Electronic Phenomena at Complex Oxide Interfaces: Insights from First Principles, *J. Phys.: Condens. Matter* **32**, 043001 (2010).
[4] Zubko, P., *et al.*, Interface Physics in Complex Oxide Heterostructures, *Annu. Rev. Condens. Matter Phys.* **2**, 141 (2011).
[5] Chaloupka, J. and Khaliullin, G., Orbital Order and Possible Superconductivity in $LaNiO_3/LaMO_3$ Superlattices, *Phys. Rev. Lett.* **100**, 016404 (2008).
[6] Middey, S., *et al.*, Epitaxial growth of (111)-oriented $LaAlO_3/LaNiO_3$ ultra-thin superlattices, *Appl. Phys. Lett.* **101**, 261602 (2012).
[7] Gibert, M., Zubko, P., Scherwitzl, R., & Triscone, J.-M. Exchange bias in $LaNiO_3/LaMnO_3$ superlattices, *Nat. Mater.* **11**, 195 (2012).
[8] Haldane, F. D. M., Model for a Quantum Hall Effect without Landau Levels: Condensed-Matter Realization of the "Parity Anomaly", *Phys. Rev. Lett.* **61**, 2015 (1988).
[9] C. Kane & E. Mele, Quantum Spin Hall Effect in Graphene, *Phys. Rev. Lett.* **95**, 226801 (2005).
[10] Raghu, S., Qi, X.-L., Honerkamp, C. & Zhang, S.-C., Topological Mott Insulators, *Phys. Rev. Lett.* **100**, 156401 (2008).
[11] Wright, A. R., Realising Haldane's vision for a Chern insulator in buckled lattices, *Sci. Rep.* **3**, 2736 (2013).
[12] Xiao, D. *et al.*, Interface engineering of quantum Hall effects in digital transition metal oxide heterostructures, *Nature Commun.* **2**, 596 (2011).
[13] Yang, K.-Y., *et al.*, Possible interaction driven topological phases in (111) bilayers of $LaNiO_3$, *Phys. Rev. B* **84**, 201104(R) (2011).

[14] Rüegg, A., & Fiete, G. A., Topological Insulators from complex orbital order in transition-metal oxides heterostructures, *Phys. Rev. B* **85**, 245131 (2011).

[15] Cook, A. M. and Paramekanti, A., Double perovskite heterostructures: magnetism, Chern bands, and Chern insulators, *Phys. Rev. Lett.* **113**, 077203 (2014).

[16] Lado, J. L., Pardo, V. & Baldomir, D., Ab initio study of Z_2 topological phases in perovskite (111) $(SrTiO_3)_7/(SrIrO_3)_2$ and $(KTaO_3)_7/(KPtO_3)_2$ multilayers, *Phys. Rev. B* **88**, 155119 (2013).

[17] Doennig, D., Pickett, W. E. & Pentcheva, R., Massive Symmetry Breaking in $LaAlO_3/SrTiO_3$(111) Quantum Wells: A Three-Orbital, Strongly Correlated Generalization of Graphene, *Phys. Rev. Lett.* **111**, 126804 (2013).

[18] Rüegg, A., Mitra, C., Demkov, A. A. & Fiete, G. A., Electronic structure of $(LaNiO_3)_2/(LaAlO_3)_N$ heterostructures grown along [111], *Phys. Rev. B* **85**, 245131 (2012).

[19] Doennig, D., Pickett, W. E. & Pentcheva, R., Confinement-driven Transitions between Topological and Mott Phases in $(LaNiO_3)_N/(LaAlO_3)_M$(111) Superlattices, *Phys. Rev. B* **89**, 121110 (2014).

[20] Rüegg, A., Mitra, C., Demkov, A. A. & Fiete, G. A., Lattice distortion effects on topological phases in $(LaNiO_3)_2/(LaAlO_3)_N$ heterostructures grown along the [111] direction, *Phys. Rev. B*, 115146 (2013).

[21] Okamoto, S., Doped Mott Insulators in (111) Bilayers of Perovskite Transition-Metal Oxides with a Strong Spin-Orbit Coupling, *Phys. Rev. Lett.* **110**, 066403 (2013).

[22] Blaha, P., Schwarz, K., Madsen, G. K. H., Kvasnicka, D. & Luitz, J., *WIEN2k, An Augmented Plane Wave Plus Local Orbitals Program for Calculating Crystal Properties*, ISBN 3-9501031-1-2 (Vienna University of Technology, Vienna, Austria, 2001).

[23] Perdew, J. P., Burke, K. & Ernzerhof, M., Generalized Gradient Approximation Made Simple, *Phys. Rev. Lett.* **77**, 3865 (1996).

[24] Anisimov, V. I., Zaanen, J., and O. K. Andersen, Band theory and Mott insulators: Hubbard U instead of Stoner I. *Phys. Rev. B* **44**, 943 (1991).

[25] Tran, F. & Blaha, P., Accurate Band Gaps of Semiconductors and Insulators with a Semilocal Exchange-Correlation Potential, *Phys. Rev. Lett.* **102**, 226401 2009.

[26] Arima, T., Tokura, Y. & Torrance, J. B., Variation of optical gaps in perovskite-type 3 d transition-metal oxides, *Phys. Rev. B* **48**, 17006 (1993).

[27] E. Pavarini, *et al.*, Mott Transition and Suppression of Orbital Fluctuations in Orthorhombic $3d^1$ Perovskites, *Phys. Rev. Lett.* **92**, 176403 (2004).

[28] De Raychaudhury, M., Pavarini, E. & Andersen, O. K., Orbital fluctuations in he different phases of $LaVO_3$ and YVO_3, *Phys. Rev. Lett.* **99**, 126402 (2007).

[29] Hsu, H., Blaha, P. & Wentzcovitch, R. M., Ferromagnetic insulating state in tensile-strained $LaCoO_3$ thin films from LDA + U calculations, *Phys. Rev. B* **85**, 140404 (2012).

[30] M. Karppinen, *et al.*, High-pressure synthesis and thermal decomposition of $LaCuO_3$, *Matl. Sci. & Eng.* **41**, 59 (1996).

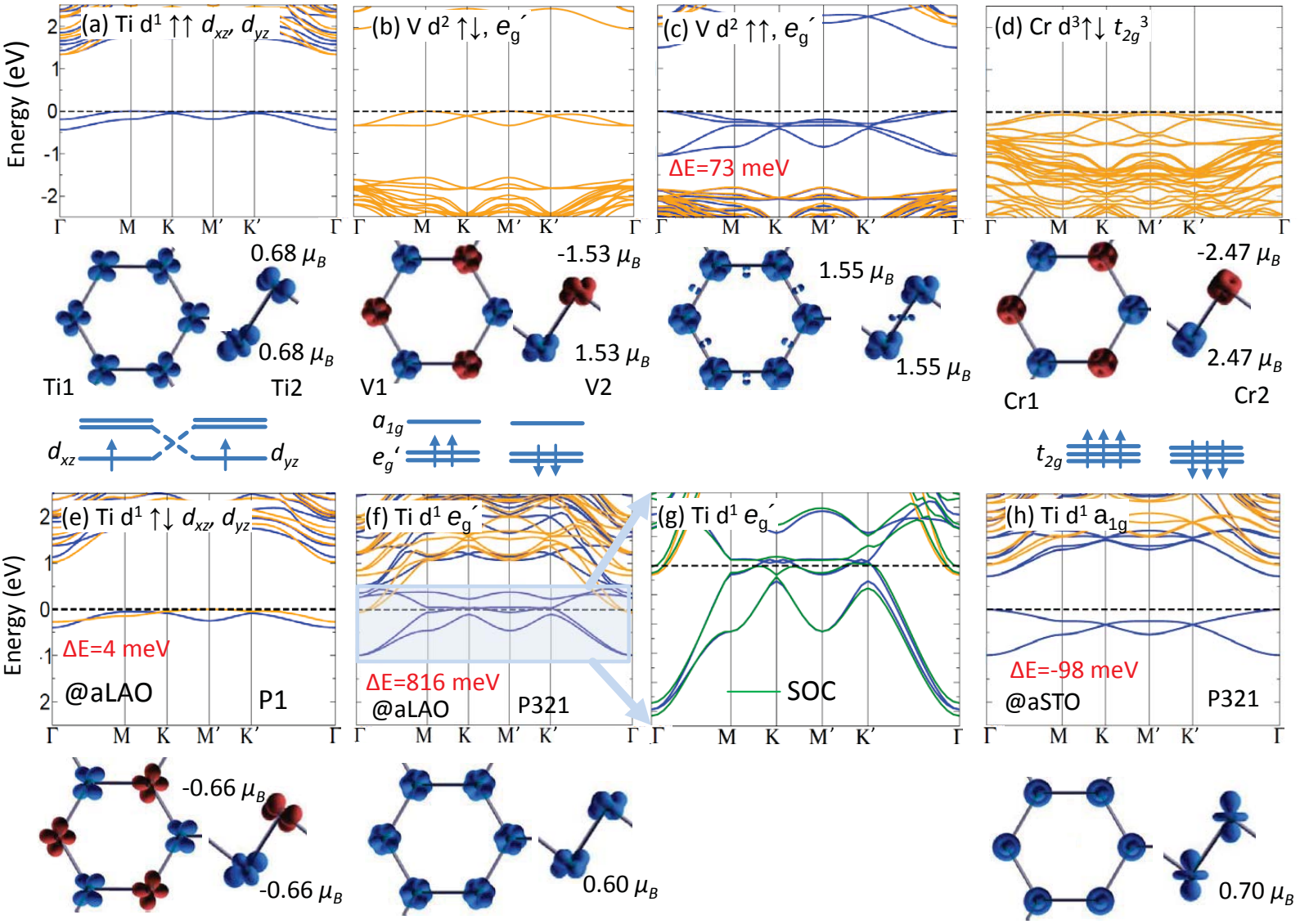
Energy (eV)
(a) Ti d¹ ↑↑ d_{xz}, d_{yz}
(b) V d² ↑↓, e_g'
(c) V d² ↑↑, e_g'
(d) Cr d³↑↓ t_{2g}^3
ΔE=73 meV
Γ M K M' K' Γ
0.68 μ_B
0.68 μ_B
Ti1
Ti2
-1.53 μ_B
1.53 μ_B
V1
V2
1.55 μ_B
1.55 μ_B
-2.47 μ_B
2.47 μ_B
Cr1
Cr2
d_{xz}
d_{yz}
a_{1g}
e_g'
t_{2g}
(e) Ti d¹ ↑↓ d_{xz}, d_{yz}
(f) Ti d¹ e_g'
(g) Ti d¹ e_g'
(h) Ti d¹ a_{1g}
ΔE=4 meV
@aLAO
P1
ΔE=816 meV
@aLAO
P321
SOC
ΔE=-98 meV
@aSTO
P321
-0.66 μ_B
-0.66 μ_B
0.60 μ_B
0.70 μ_B

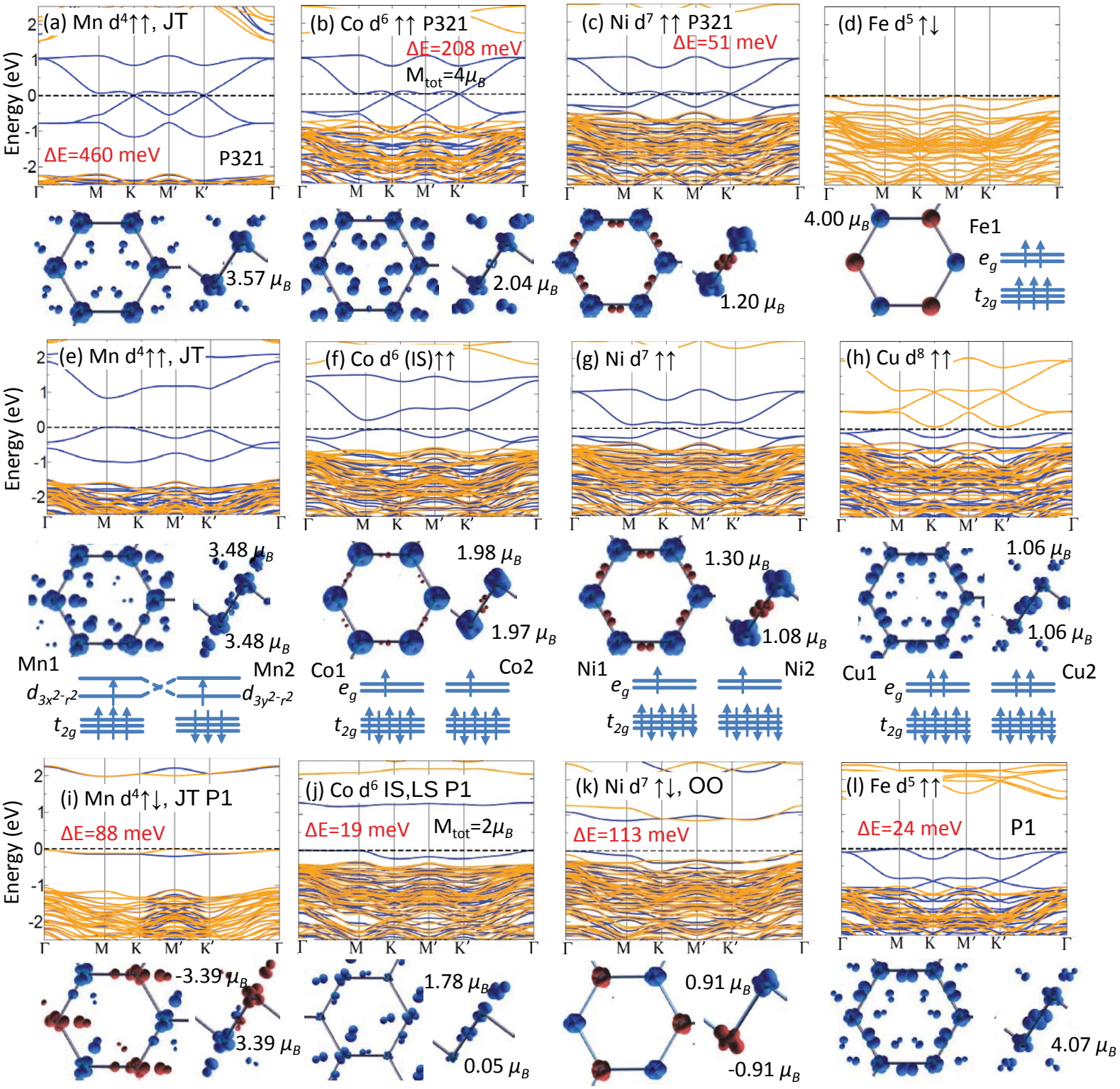
(a) Mn d⁴↑↑, JT
ΔE=460 meV
P321
(b) Co d⁶ ↑↑ P321
ΔE=208 meV
M_tot=4μ_B
(c) Ni d⁷ ↑↑ P321
ΔE=51 meV
(d) Fe d⁵ ↑↓
Energy (eV)
Γ M K M' K' Γ
3.57 μ_B
2.04 μ_B
1.20 μ_B
4.00 μ_B
Fe1
e_g
t_2g
(e) Mn d⁴↑↑, JT
(f) Co d⁶ (IS)↑↑
(g) Ni d⁷ ↑↑
(h) Cu d⁸ ↑↑
3.48 μ_B
3.48 μ_B
1.98 μ_B
1.97 μ_B
1.30 μ_B
1.08 μ_B
1.06 μ_B
1.06 μ_B
Mn1
Mn2
d_3x²-r²
d_3y²-r²
t_2g
Co1
Co2
e_g
Ni1
Ni2
Cu1
Cu2
(i) Mn d⁴↑↓, JT P1
ΔE=88 meV
(j) Co d⁶ IS,LS P1
ΔE=19 meV
M_tot=2μ_B
(k) Ni d⁷ ↑↓, OO
ΔE=113 meV
(l) Fe d⁵ ↑↑
ΔE=24 meV
P1
-3.39 μ_B
3.39 μ_B
1.78 μ_B
0.05 μ_B
0.91 μ_B
-0.91 μ_B
4.07 μ_B

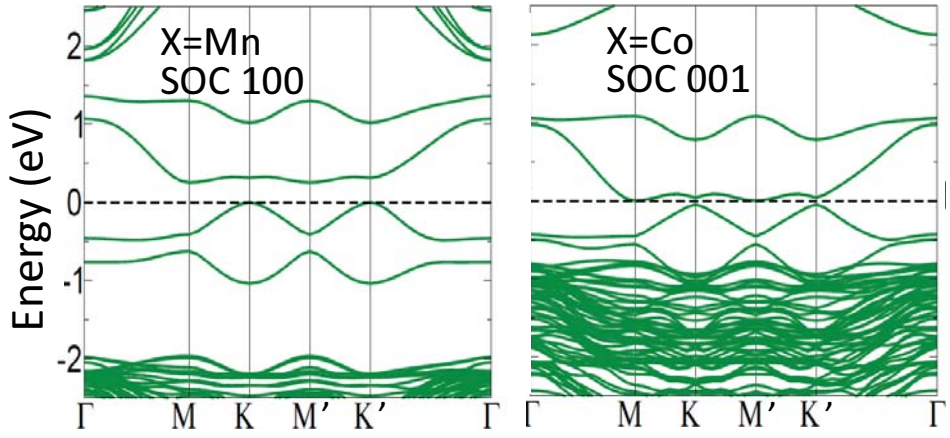
X=Mn
SOC 100
X=Co
SOC 001
Energy (eV)
2
1
0
-1
-2
Γ
M
K
M'
K'
Γ
Γ
M
K
M'
K'
Γ